Chin. J. Astron. Astrophys. Vol. 4 (2004), No. 5, 427–439
(http://www.chjaa.org or http://chjaa.bao.ac.cn)

Chinese Journal of Astronomy and Astrophysics

Chandra Observations of the Flat Spectrum Seyfert-2 Galaxies NGC 2110 and NGC 7582 *

Hui Dong[1], Sui-Jian Xue[2], Cheng Li[1] and Fu-Zhen Cheng[1]

[1] Center for Astrophysics, University of Science and Technology of China, Hefei 230026; donghui@mail.ustc.edu.cn

[2] National Astronomical Observatories, Chinese Academy of Sciences, Beijing 100012

Received 2004 February 18; accepted 2004 July 5

Abstract *Chandra* observations of the Seyfert-2 galaxies NGC 2110 and NGC 7582 are presented. With the superb spatial resolution of *Chandra* we found that in NGC 7582 the soft ($\leq$2 keV) and hard (2–10 keV) X-rays are emitted in different regions, consistent with the report by Xue et al. By comparing the present X-ray data with the previous infrared data, we determined that the soft X-ray region is the site of starburst activities. We found no significant temporal variations during our observations. We confirm the previous finding that NGC 2110 and NGC 7582 are flat-spectrum sources. We argue that the flat spectra may result from a cold absorbing material such as envisaged in the "dual absorbed" model. Strong Fe K_α emission feature is detected in 6$\sim$7 keV. Its equivalent width is so large that it cannot be reproduced by using the Galactic column density of $\sim 10^{22}$ cm^{-2}.

Key words: X-rays: image — X-ray: spectrum — Galaxy: Seyfert — Galaxy: individuals: NGC 7582 and NGC 2110

1 INTRODUCTION

By analyzing some *Ginga* samples of Seyfert-1 galaxies, Nandra & Pounds (1994) and Pounds et al. (1990) found that when both reflection and ionized absorption were taken into account, the intrinsic power-law spectra of Seyfert-1s had a mean photon index of $\Gamma = 1.9$–2.0. This value has been confirmed by Haardt & Maraschi (1991, 1993) using a two-phase accretion disk model within the unified Seyfert scenario, in which thermal Comptonization is the basic mechanism for producing the observed X-ray power-law continuum. The model was also applied by Haardt (1993) and Ueda, Ebisawa & Done (1994) to the spectra of several Galactic black hole candidates, and by Zdziarski et al. (1994) to IC 4329A. In terms of the unified Seyfert theory, Seyfert-2s and Seyfert-1s have the same intrinsic nuclear properties, so Seyfert-2s are expected to have $\Gamma \sim 1.9 - 2.0$, too. However, the *Ginga*, *ASCA* and *BeppoSAX* observations have shown many cases where the intrinsic spectra of Seyfert-2s are much flatter and many other cases where they are even steeper than $\Gamma \sim 2$, notwithstanding the use of complicated models (e.g. Smith & Done 1996; Turner et al. 1997). The steeper spectra may be explained relatively

* Supported by the National Natural Science Foundation of China.

easily by the radiative transfer effects. On the other hand, the observed flatter spectra cannot be explained by the theory of Haardt (Smith & Done 1996). If these spectra are intrinsically flat, we may need to revise the current standard unified Seyfert theories and Haardt's two-phase accretion disk model. Moreover, it is still possible that the flat-spectrum is important for understanding the nature of the X-ray background. As stated in Zdziarski et al. (1995), the flat-spectrum sources may contribute significantly to the high energy end of the background, while the steep-spectrum sources may dominate at lower energies.

To date the results of only a few X-ray observations of the flat-spectrum Seyfert-2s (Cappi et al. 1996; Vignali et al. 1998; Malizia et al. 1999; Malagati et al. 1999) are consistent with the unified Seyfert theories. In these works the authors either introduced a complex absorption or added a reflection component in their model. In every single case, it was assumed that the spectrum was intrinsically steep, which turned out to be flat either due to extremely heavy absorption in soft X-rays or due to reflection enhancement in hard X-rays.

In this paper, we present the *Chandra* observations of two typical flat-spectrum Seyfert-2s, NGC 2110 and NGC 7582. The two sources were first identified as X-ray sources with the HEAO-1/SMC instrument, and were classified as Seyfert-2s because their optical spectra showed no broad emission lines. They are also known as prototype Narrow Emission Line Galaxies (NELGs), a transition class between Seyfert-1s and Seyfert-2s (e.g. Lawrence & Elvis 1982), because of their relatively strong emission in 2–10 keV (intrinsic L_x estimated to be $\sim 10^{42} - 10^{43}$ erg s^{-1}). According to their previous X-ray studies (Mushotzky 1982; Maccacaro & Perola 1981; Turner et al. 1991; Turner & Pounds 1989; Smith & Done 1996; Turner et al. 1998 ; Risaliti 2002), their 2–10 keV spectra show a constant flat shape, with averaged photon indices 1.69 and 1.4 for NGC 2110 and NGC 7582, respectively. In 1998, Xue at al. reported a significant variation in the absorption column density of NGC 7582 ($\Delta N_{\rm H}\sim 4 \times 10^{22}$ cm^{-2}) after comparing two *ASCA* observations, one of 1994 and one of 1996. They also found that the variability was different in the hard and soft X-rays: highly variable in the hard X-rays, while almost no variability in the soft X-rays.

This paper is organized as follows. The observations and data reduction are described in Sect. 2. The results of the temporal analysis are presented in Sect. 3. The results of the image and spatial analysis are presented in Sect. 4. Finally, our conclusions are given in Sect. 5.

2 OBSERVATIONS AND DATA REDUCTION

NGC 2110 was observed with the *Chandra* ACIS cameras four times and NGC 7582, twice (Table 1). The observations were made in the very faint (VFAINT) mode. The data had first been processed with the pipeline SDP before they were made available to the public. The most updated calibration files, including ACIS QEU, gain map, bad pixel lists and others, were used in the data reduction. The data were filtered to include only standard *ASCA* event grades 2, 3, 4 and 6.

The pre-processed and astrometrically-aligned data products were then analyzed with the standard CIAO package (version 2.3). An inspection of bad aspect times and high background times was carried out. A significant background flare event that lasting $\sim$ 5840s was detected during the observation #436. To avoid the effect of this background flare, we divided this observation into two parts, #436A and #436B, and analysed the two parts separately. After removing all time intervals with large background count rates, we have an effective exposure time of 17.5 ks for #3143, 17.4 ks for #3417, 40.9 ks for #3418, 4.7 ks for #436A, 2.7 ks for

#436B and 4.9 ks for #2319. Our analysis was restricted to the energy range 0.3–10 keV.

Table 1 *Chandra* Observation Log

Source	Obs_ID	Exposure (ks)	Frame Time (s)	Date
NGC 2110	883	50	0.4	4/22/2000
NGC 2110	3143	35	3.2	12/19/2001
NGC 2110	3417	35	3.2	12/22/2001
NGC 2110	3418	80	3.2	12/20/2001
NGC 7582	436	13	3.2	10/14/2000
NGC 7582	2319	7	3.2	10/15/2000

As stated in Table 1, the observations used in this paper were made with a frame time of 3.2 s, so that the inner regions of the galaxies may have been affected by the pile-up effect. The common method used to determine the significance of the pile-up effect is to compare the count rates made with frame time 3.2 s with those of 0.1 s or 0.4 s (alternating mode, Davis 2001). For NGC 2110, because the previous observations did not show any meaningful variability in its X-ray flux, we used the observation #883 to examine the pile-up effect on observations #3143, #3417, and #3418. The count rate of #883 is nearly twice the rate of other three, implying that the latter three suffered significantly from the pile-up effect. The fractions of the pile-up photons are estimated to be 50.2%, 47.8% and 50.7%, respectively. The only method to correct the pile-up effect is to eliminate the photons from the center of NGC 2110. In this paper, we were precluded from doing this because we did not want to lose information from the galaxy center, so we included the photons from the brightest region in our analysis. For NGC 7582, there is no observations performed in the alternating mode. However, the 2–10 keV flux of NGC 7582 obtained with *Chandra* (0.78×10^{-11} erg cm^{-2} s^{-1}) was comparable to the previous results (*BeppoSAX*: 1.5×10^{-11} erg cm^{-2} s^{-1}, Turner et al. 2000; *ASCA*: 1.39×10^{-11} erg cm^{-2} s^{-1}, Turner et al. 1997; *Ginga*: 0.6×10^{-11} erg cm^{-2} s^{-1}, Warwick et al. 1993), indicating that the two observations of NGC 7582 might be almost free of the pile-up effect. There is a bright streak across the center of NGC 2110 in the observation #883. We tried to remove it with the CIAO tool acisreadcorr but it still remained. So we did not use this observation in the following analysis. The basic data of NGC 2110 and NGC 7582 taken from the literature are shown in Table 2.

Table 2 Basic Data of NGC 7582 and NGC 2110

Name	R. A. J2000	Decl.	z	Class	$N_{\rm H}^{\rm a}$
NGC 2110	$05^{\rm h}\ 52^{\rm m}\ 11.4^{\rm s}$	$-07^\circ 27' 22''$	0.0078	S2/NELG	18.60
NGC 7582	$23^{\rm h}\ 18^{\rm m}\ 23.5^{\rm s}$	$-42^\circ 22' 11''$	0.0053	S2/NELG	1.47

[a] The Galactic column density is quoted from Stark et al. (1992) in 10^{20} cm^{-2}.

3 TEMPORAL ANALYSIS

To check the variability in the X-ray flux of NGC 2110 and NGC 7582, we constructed their light curves for each observation, using the CIAO software (version 2.3). We extracted the 0.3–10 keV light-curves from the central 10″ regions of the galaxies. The size of each bin

was set to be 250 s, so there were more than 25 counts in each bin. No significant variability was found in each observation. We have performed χ^2 tests to examine if the X-ray flux is constant. The results are listed in Table 3. It can be clearly seen that the light curves are well fitted with a constant. Since some previous observations show that the two objects are highly variable in 2–10 keV, we then extracted separate light-curves in 0.3–2 keV and 2–10 keV and repeated our examination. Again we found no major temporal variations.

It should be noted that the statement may be unreliable that NGC 7582 showed no variability in its flux during the *Chandra* observations, because the total exposure time for NGC 7582 was short ($\leq$5000 s). As for NGC 2110, although a rapid variability was expected, the results of the previous X-ray observations were mutually conflicting: with *Ginga*, Polletta et al. (1996) and Hayashi et al. (1996) found a significant variability in 2–10 keV, while with *ASCA* Turner et al. (1997) and Hayashi et al. (1996) found no rapid variability.

Table 3 Results of the Temporal Analysis

Obs_ID	3143	3417	3418	436a	436b	2319
χ^2/dof	0.505/132	0.496/131	1.063/300	0.071/18	0.110/11	0.095/18

4 X-RAY IMAGING ANALYSIS

Figure 1 shows the 0.3–10 keV X-ray contours of NGC 2110 and NGC 7582, overlaid on their optical DSS images. Figure 2 and Fig. 3 show the nuclear regions of NGC 2110 and NGC 7582 in three different bands (0.3–1 keV, 1–3 keV and 3–10 keV). These images were smoothed using the CIAO tool *csmooth* at 3σ significant levels. The smoothing function was a scale-variable 2-dimensional Gaussian with a maximum scale of 10 pixels ($\approx 5''$) to avoid over-smoothing. The small circle (radius $2''$) in each panel marks the position of the hard X-ray center. It is obvious that for both objects the hard X-ray emissions originate from a compact region while the soft X-ray emissions come from a diffuse halo and bright complex structures. As can be seen in Fig. 2, there seems to be changes in the X-ray morphology between the different bands for NGC 2110. This phenomenon, however, might be due to the pile-up effect, since the three observations of NGC 2110 are less than two days apart.

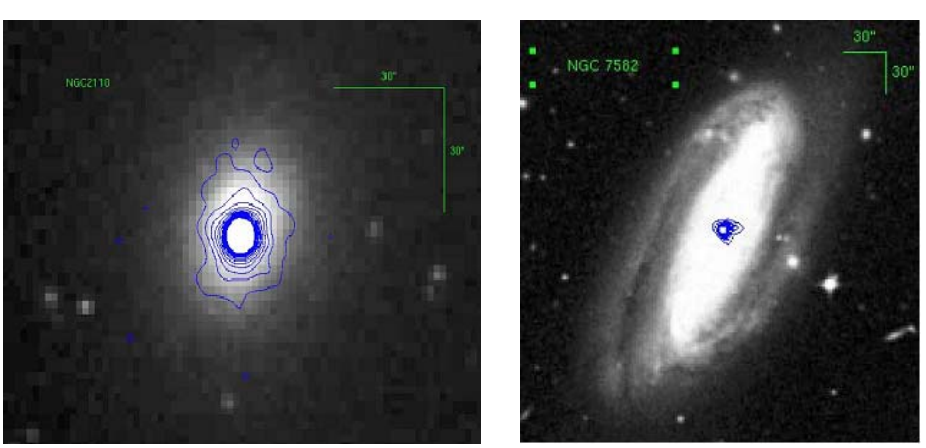

Fig. 1 Optical images of NGC7582 and NGC 2110.

In NGC 7582 the central emission region shown in the soft X-rays is quite different from that in the hard X-rays (Fig. 3). They have different centers, separated by about 300 pc (H_0=50 km s^{-1} Mpc^{-1}), indicating that the soft and hard X-rays are emitted from different regions, and this is consistent with the conclusion of Xue et al. (1998). Also, we argue that the soft and hard X-ray emissions in NGC 7582 might have different physical origins. By studying the optical spectrum of NGC 7582, Ward et al. (1980) showed there is a significant population of hot stars in its central region and in the infrared spectrum Roche et al. (1984) found both dust emission and silicate absorption features. So it can be inferred that violent starburst activities are going on in the central region of NGC 7582. We therefore speculate that, in NGC 7582, the soft X-rays are emitted from the extended starburst regions, while the hard X-rays are from the active nuclear region.

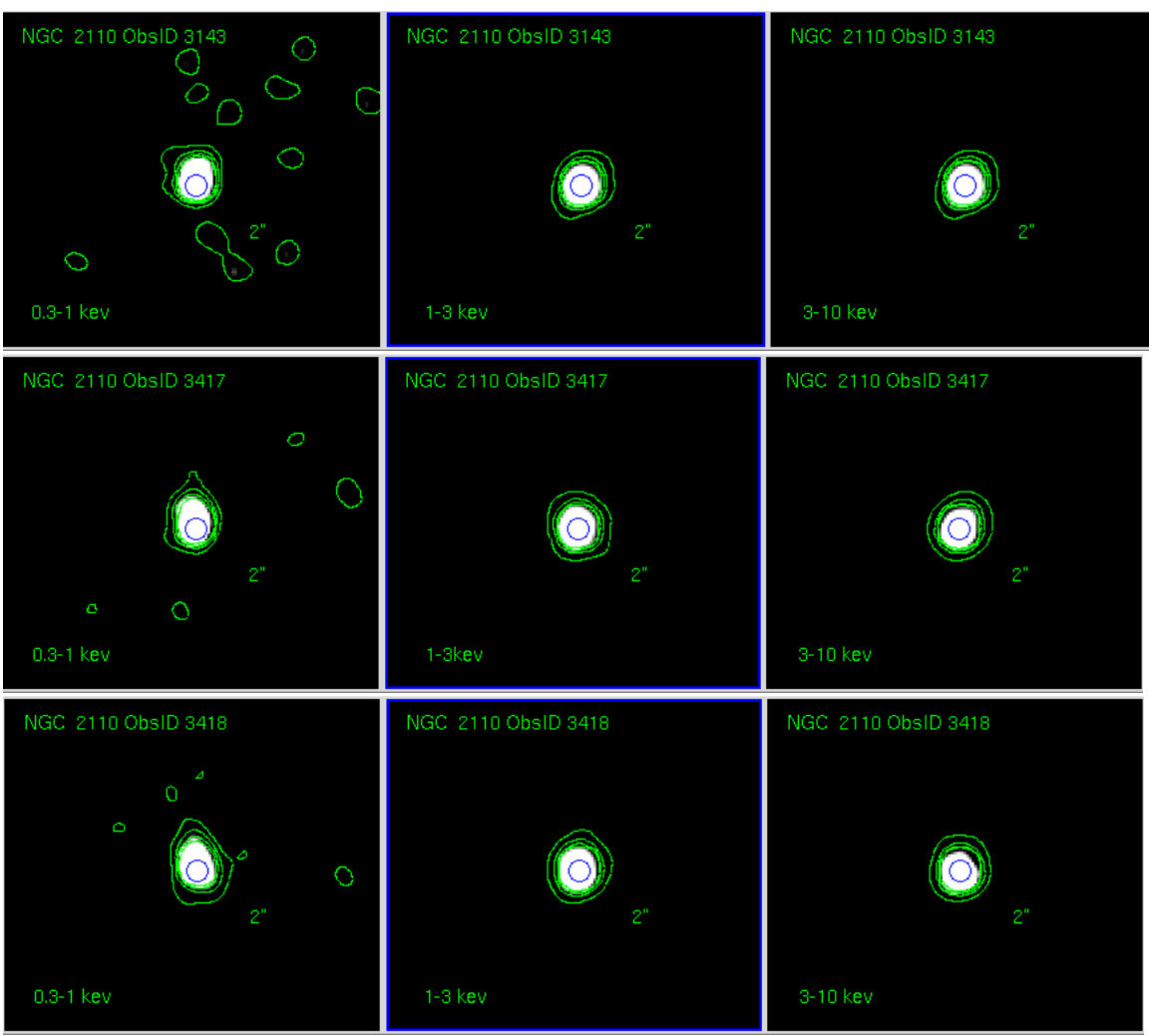

Fig. 2 Central region of NGC 2110 in different energy bands.

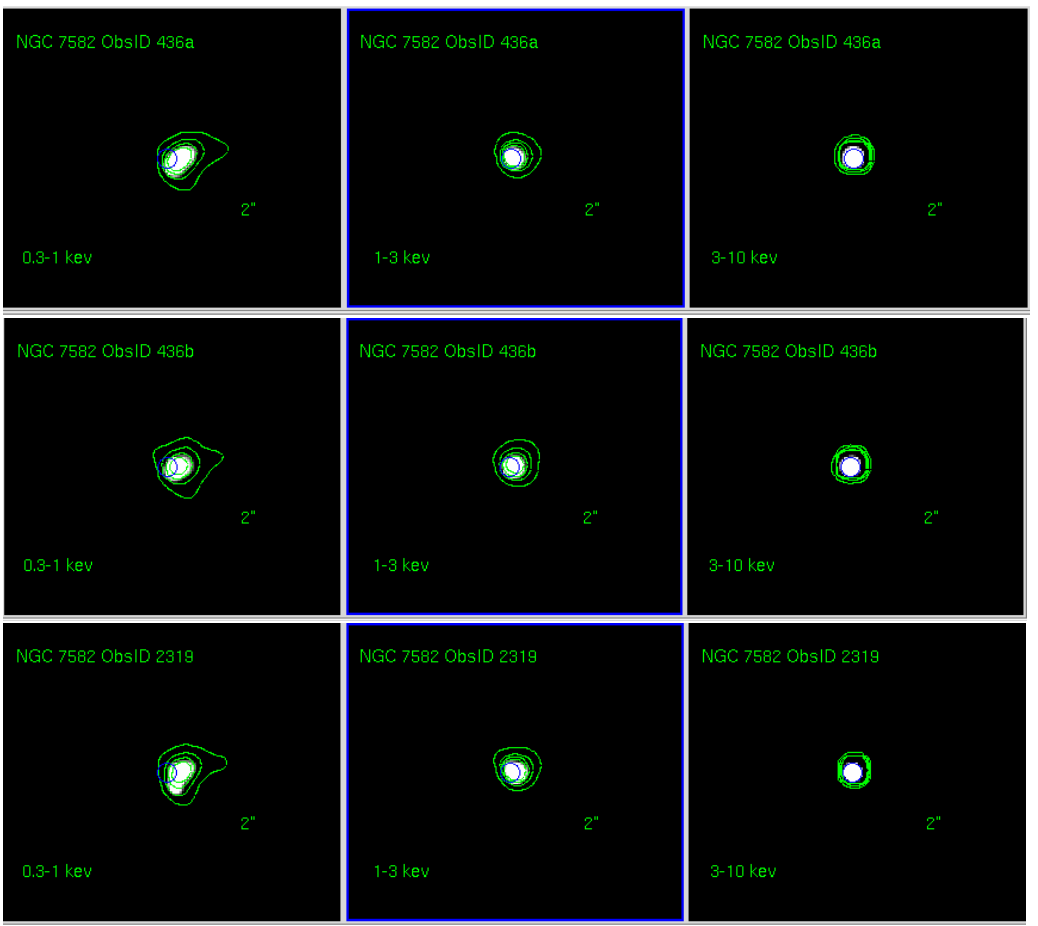

Fig. 3 Central region of NGC 7582 in different energy bands.

5 X-RAY SPECTRAL ANALYSIS

Spectra were extracted from the two circle regions of diameter $10''$ centered on the nuclei of the two galaxies and were grouped to have at least 15 photons per energy bin to allow the use of the χ^2 test. The spectra were then analyzed using the XSPEC software (version 11.2.0). The error bars were calculated for the 90% confidence level.

To check whether our data are consistent with the previous X-ray data, we first fitted the spectra with a simple absorbed power-law model. The goodness of fit here is poor (Table 4). For NGC 7582, the data exceed the model in the bins < 2 keV, 4–5 keV, and 6–7 keV where the iron K emission lines are expected. For NGC 2110, there is also a line feature in 6–7 keV besides the emission excess at $\sim$2.3 keV. The excess at lower energies is not seen in NGC 2110. The obtained photon indices are too small, which might partly be due to the pile-up effect, or due to the existence of a soft X-ray component, as was seen in NGC 7582.

Therefore, we concentrated on the 3–8 keV spectra and, after excluding the Fe K_α lines, fitted the spectra again with the absorbed power-law model. The best-fit photon index is now increased to 0.2513 (for #3143), 0.1637 (#3417), 0.2518 (#3418), 1.354 (#436) and 1.238 (#2319). For NGC 7582, the photon indices are consistent with those from the previous observations, while for NGC 2110 the photon indices are still too small, this is probably due to the pile-up effect.

Then we fitted the spectra including those parts ignored at lower energies. In order to improve the quality of the fitting, we tried adding another possible spectral component: to account for the excess below 2 keV that might be due to the emission of a warm gas induced by starburst activities, we added a thermal Raymond-Smith component. For NGC 7582, the best-fit temperature of this additional thermal component was found to be $\simeq$0.76 keV (Table 5), and with this model, only a few residuals remained in 0.8–1 keV. For NGC 2110, this addition did not significantly improve the fit.

Table 4 Power-law Fits to the Observed Spectra

#	A_{pl}^{a}	Γ	N_H^{b} (10^{22} cm^{-2})	Flux^{c} ($2-10$ keV)	χ^2_ν/dof
3143	$8.355^{+0.214}_{-0.208}$	$0.46^{+0.02}_{-0.02}$	$1.15^{+0.11}_{-0.10}$	2.62	309/220
3417	$7.676^{+0.196}_{-0.196}$	$0.42^{+0.02}_{-0.01}$	$0.98^{+0.11}_{-0.09}$	2.60	287/219
3418	$8.028^{+0.134}_{-0.134}$	$0.45^{+0.02}_{-0.02}$	$1.09^{+0.07}_{-0.06}$	2.57	611/403
436	0.317	–0.69	0	0.90	649/135
2319	0.237	–0.88	0	0.99	446/72

[a] Flux at 1 keV in units of 10^{-4} photons cm^{-2} s^{-1} keV^{-1};

[b] Total absorption column density;

[c] 2–10 keV flux in units of 10^{-11} erg cm^{-2} s^{-1}.

Table 5 Spectral Fit with the Model that Includes a Power-law and a Raymond-Smith Component

#	A_{pl}^{a}	Γ	N_H^{b} (10^{22} cm^{-2})	kT (keV)	Abundance (solar)	Flux^{c} ($2-10$keV)	χ^2_ν/dof
3143	$9.186^{+0.232}_{-0.233}$	$0.52^{+0.01}_{-0.01}$	$1.29^{+0.11}_{-0.11}$	$0.35^{+0.11}_{-0.11}$	$0.26^{+0.15}_{-0.16}$	2.59	301/217
3417	$8.950^{+0.229}_{-0.229}$	$0.51^{+0.02}_{-0.01}$	$1.19^{+0.11}_{-0.10}$	$0.27^{+1.41}_{-0.04}$	$0.40^{+0.16}_{-0.16}$	2.61	270/216
3418	$9.301^{+0.156}_{-0.156}$	$0.54^{+0.01}_{-0.01}$	$1.31^{+0.08}_{-0.07}$	$0.77^{+0.13}_{-0.13}$	$0.21^{+0.07}_{+0.10}$	2.51	589/400
436	$2.157^{+0.103}_{-0.102}$	$0.18^{+0.03}_{-0.03}$	$8.34^{+0.71}_{-0.61}$	$0.76^{+0.05}_{-0.05}$	$0.04^{+0.01}_{-0.01}$	0.92	164/132
2319	$4.510^{+0.314}_{-0.282}$	$0.49^{+0.04}_{-0.04}$	$13.66^{+1.12}_{-1.11}$	$0.76^{+0.06}_{-0.05}$	$0.05^{+0.01}_{-0.01}$	0.92	91/69

[a] Flux of the power-law component at 1 keV in units of 10^{-4} photons cm^{-2} s^{-1} keV^{-1};

[b] Column density that does not include the Galactic contribution;

[c] Observed flux in 2–10 keV in units of 10^{-11} erg cm^{-2} s^{-1}.

Within the frame of the unified Seyfert theories there have been two possible spectral models for the observed flat spectrum of Seyfert 2s, the dual absorbed model and the reflection model. In the dual absorbed model, it is assumed that in the line of sight, besides the matter totally covering the active nucleus (e.g. accretion disk and torus), there is an additional warm matter with a hydrogen column density larger than $\sim 10^{23}$ cm^{-2}, so that in this matter Thomson scattering cannot take place efficiently and the X-ray photons at the high energy end cannot be totally absorbed. Since this matter partially covers the nucleus, it only absorbs a portion of

the soft X-ray emission and produces most of the iron K lines and edge features. In the past, the spectra of a number of flat-spectrum sources have been explained with this model, such as in Cappi et al. (1996, NGC 5252), Hayashi et al. (1996, NGC 2110), Guainazzi et al. (1998, NGC 7172). Alternatively, in the reflection model, an intrinsic steep continuum together with a reflection component that contributes to the high energy end is used to explain the observed flat spectrum.

We have attempted to examine these two models by spectral fitting. We used the PCFABS model (Magdziarz & Zdziarski 1995) to represent the dual absorbed component with a covering fraction C_f, and the pexrav model (Magdziarz & Zdziarski 1995) to represent the reflected component with the parameters abund, Fe-abund and CosIncl fixed at the default values because they were not well constrained if left free.

The best-fits of the two models are shown in Figs. 4 and 5, and Tables 6 and 7. For NGC 7582, we find that the dual absorbed model with an additional column density of $N_{\rm H} \approx 2\times10^{23}$ cm^{-2} and a photon index of $\Gamma\sim1.83$ could well fit the observed spectra. For NGC 2110, the dual absorbed model gives a good fit, too, with the photon index increased at least by 0.2. The reflection model gave poorer fits, as judged by the χ^2 test. In both cases, a narrow Gaussian line was added to allow for the Fe K$_\alpha$ line feature.

Table 6 Best-Fits with the Dual Absorbed Model

#	$A_{pl}^{\rm a}$	Γ	$N_{\rm H}^{\rm b}$	$N_{\rm H,pc}^{\rm c}$	C_f	kT	Abundance	Flux$^{\rm d}$	χ^2_ν/dof
			(10^{22} cm^{-2})		(%)	(keV)	(solar)	(2–10 keV)	
3143	$105.620^{+2.710}_{-2.620}$	$0.73^{+0.02}_{-0.02}$	$1.49^{+0.12}_{-0.11}$	$192.10^{+19.09}_{-14.27}$	$0.883^{+0.03}_{-0.03}$	–	–	2.76	291/218
3417	$483.020^{+12.794}_{-11.823}$	$0.65^{+0.02}_{-0.02}$	$1.26^{+0.11}_{-0.11}$	$305.30^{+20.39}_{-16.60}$	$0.978^{+0.0006}_{-0.0006}$	–	–	2.83	263/217
3418	$227.200^{+3.791}_{-3.792}$	$0.64^{+0.01}_{-0.01}$	$1.32^{+0.7}_{-0.7}$	$273.90^{+17.50}_{-13.41}$	$0.954^{+0.008}_{-0.0008}$	–	–	2.72	583/401
436	$40.833^{+1.937}_{-1.884}$	$1.63^{+0.03}_{-0.03}$	$4.76^{+0.55}_{-0.51}$	$20.01^{+1.36}_{-1.25}$	$0.907^{+0.014}_{-0.015}$	$0.69^{+0.04}_{-0.04}$	$0.03^{+0.01}_{-0.01}$	0.74	148/130
2319	$60.793^{+4.291}_{-3.708}$	$1.74^{+0.04}_{-0.04}$	$5.69^{+0.91}_{-0.84}$	$24.83^{+1.58}_{-2.24}$	$0.931^{+0.016}_{-0.017}$	$0.72^{+0.05}_{-0.05}$	$0.04^{+0.01}_{-0.01}$	0.76	87/67

[a] Flux of the power-law component at 1 keV in units of 10^{-4} photons cm^{-2} s^{-1} keV^{-1};

[b] Absorption column density that does not include the Galactic value;

[c] Additional column density covering a fraction C_f of the source;

[d] $2-10$ keV flux in units of 10^{-11} erg cm^{-2} s^{-1}.

Table 7 The Reflection Model

#	$A_{pl}^{\rm a}$	Γ	$N_{\rm H}^{\rm b}$		kT	Abundance	Flux$^{\rm d}$	χ^2_ν/dof
			(10^{22} cm^{-2})	$R^{\rm c}$	(keV)	(solar)	(2–10 keV)	
3143	$8.537^{+0.216}_{-0.216}$	$0.48^{+0.02}_{-0.02}$	$1.15^{+0.11}_{-0.10}$	$0.177^{+0.456}_{-0.177}$	–	–	2.62	309/218
3417	$8.276^{+0.209}_{-0.213}$	$0.49^{+0.02}_{-0.02}$	$1.02^{+0.10}_{-0.10}$	$0.549^{+0.473}_{-0.078}$	–	–	2.59	287/217
3418	$9.069^{+0.156}_{-0.147}$	$0.55^{+0.02}_{-0.01}$	$1.18^{+0.07}_{-0.07}$	$0.763^{+0.326}_{-0.309}$	–	–	2.54	611/401
436	$0.238^{+0.011}_{-0.011}$	$0.90^{+0.03}_{-0.03}$	$1.68^{+0.43}_{-0.37}$	$569.7^{+28.8}_{-27.1}$	$0.87^{+0.02}_{-0.02}$	$0.21^{+0.02}_{-0.02}$	0.79	166/130
2319	$0.204^{+0.014}_{-0.013}$	$0.895^{+0.041}_{-0.041}$	$1.45^{+0.66}_{-0.55}$	$426.6^{+31.3}_{-27.9}$	$0.86^{+0.03}_{-0.03}$	$0.28^{+0.03}_{-0.04}$	0.94	100/67

[a] Flux of the power-law component at 1 keV in units of 10^{-4} photons cm^{-2} s^{-1} keV^{-1} in the observer's frame;

[b] Absorption column density that does not include the Galactic value;

[c] Reflection scaling factor;

[d] Observed flux in 2–10 keV in units of 10^{-11} erg cm^{-2} s^{-1}.

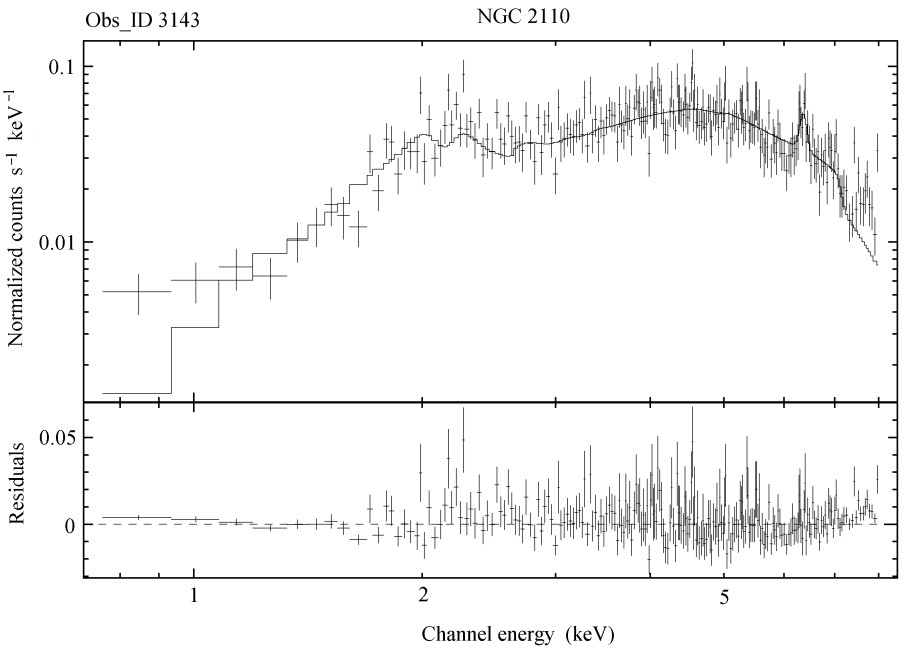

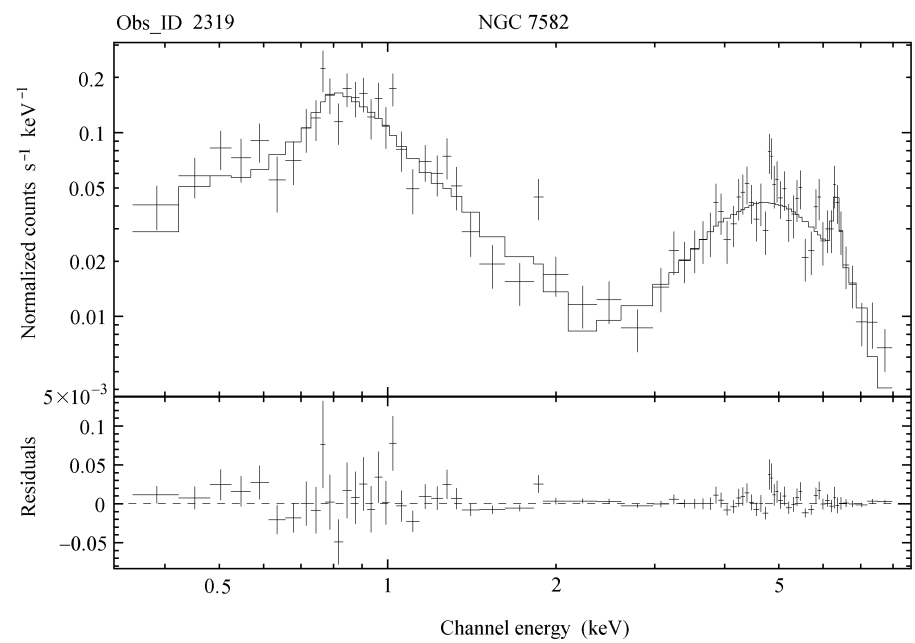

Fig. 4 Dual absorbed model plus the Fe K$_\alpha$ line.

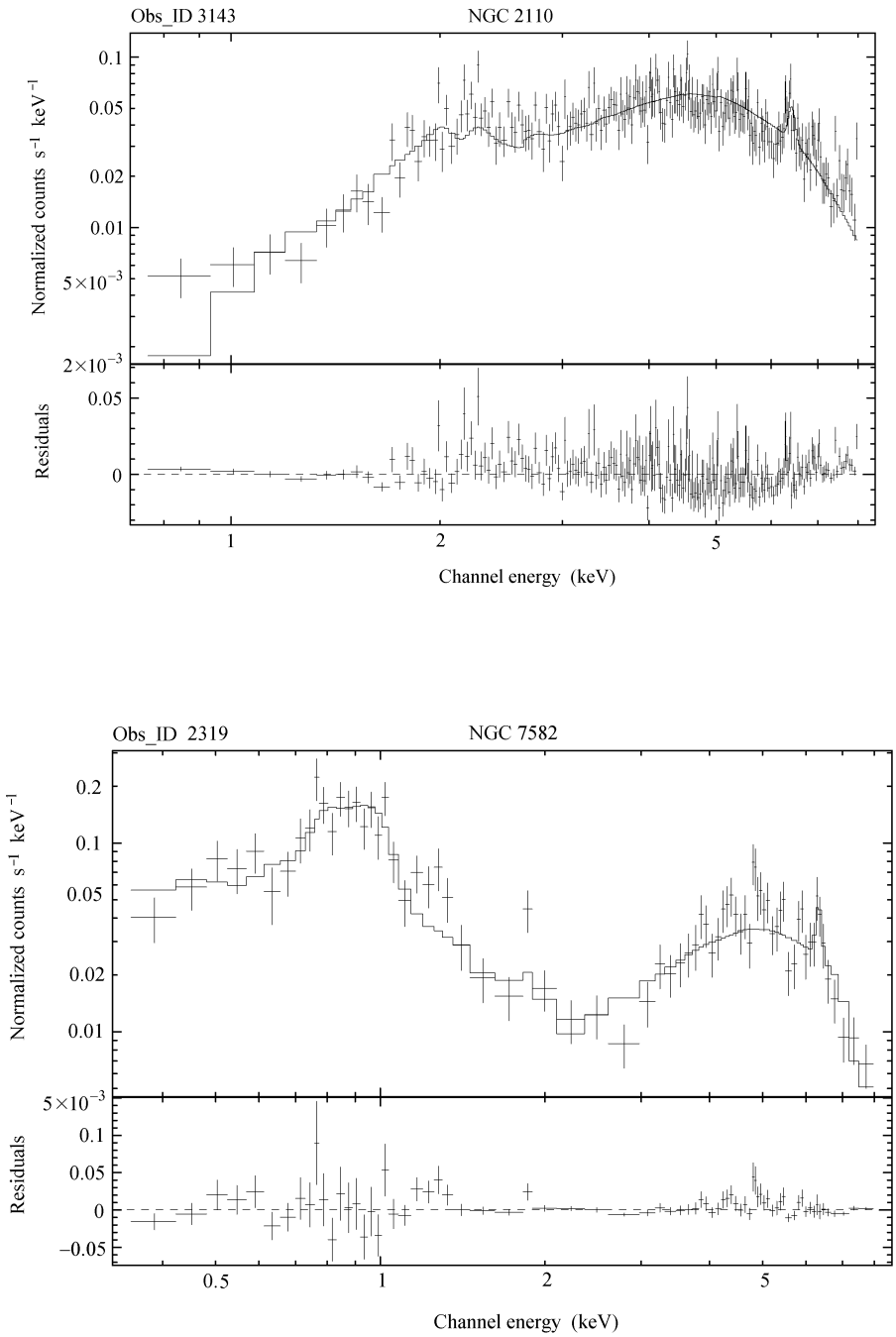

Fig. 5 Reflection model plus the Fe K$_\alpha$ line.

Table 8 The Best-fitting Results with the Dual Absorbed Model Plus the Fe K$_\alpha$ Lines

#	Γ	$N_{\rm H}^{\rm a}$	$N_{\rm H,pc}^{\rm b}$	C_f	kT	Abundance	$E_{\rm K\alpha}$	EW	Flux[c]	χ^2_ν/dof
		(10^{22} cm^{-2})		(%)	(keV)	(solar)	(keV)	(eV)		
3143	$0.73^{+0.02}_{-0.02}$	$1.49^{+0.12}_{-0.11}$	$206.10^{+25.25}_{-15.91}$	$0.884^{+0.0030}_{-0.0031}$	–	–	$6.341^{+0.037}_{-0.031}$	$96.6^{+9.4}_{-22}$	2.71	276/215
3417	$0.67^{+0.02}_{-0.02}$	$1.28^{+0.11}_{-0.11}$	$271.10^{+23.28}_{-14.55}$	$0.963^{+0.0009}_{-0.0010}$	–	–	$6.316^{+0.073}_{-0.074}$	$41.2^{+37.5}_{-34.7}$	2.79	261/214
3418	$0.61^{+0.01}_{-0.01}$	$1.28^{+0.07}_{-0.07}$	$408.10^{+26.17}_{-18.77}$	$0.991^{+0.001}_{-0.0002}$	–	–	$6.354^{+0.032}_{-0.031}$	$78.3^{+27.7}_{-26.5}$	2.69	568/398
436	$1.85^{+0.03}_{-0.03}$	$4.95^{+0.56}_{-0.50}$	$20.38^{+1.28}_{-1.22}$	$0.918^{+0.013}_{-0.014}$	$0.69^{+0.05}_{-0.04}$	$0.3^{+0.01}_{-0.01}$	$6.353^{+0.064}_{-0.072}$	$128.0^{+92.0}_{-75.0}$	0.74	148/130
2319	$1.83^{+0.04}_{-0.05}$	$5.52^{+0.94}_{-0.80}$	$23.27^{+1.72}_{-1.88}$	$0.936^{+0.016}_{-0.016}$	$0.72^{+0.05}_{-0.05}$	$0.04^{+0.01}_{-0.01}$	$6.321^{+0.059}_{-0.054}$	$260.0^{+131.0}_{-134.0}$	0.76	77/64

[a] Absorption column density that does not include the Galactic contribution;

[b] Additional column density covering a fraction C_f of the source;

[c] Observed flux in 2–10 keV in units of 10^{-11} erg cm^{-2} s^{-1}.

Table 9 The Reflection Model Plus the Contribution of Fe K$_\alpha$ Lines

#	Γ	$N_{\rm H}^{\rm a}$	$R^{\rm b}$	kT	Abundance	$E_{\rm K\alpha}$	EW	Flux[c]	χ^2_ν/dof
		(10^{20} cm^{-2})		(keV)	(solar)	(keV)	(eV)		
3143	$0.53^{+0.02}_{-0.02}$	122^{+11}_{-10}	< 0.411	–	–	$6.348^{+0.032}_{-0.033}$	$127.0^{+45.0}_{-44.5}$	2.58	288/215
3417	$0.45^{+0.02}_{-0.01}$	100^{+10}_{-10}	$1.33^{+0.431}_{-1.33}$	–	–	$6.328^{+0.067}_{-0.064}$	$58.6^{+38.5}_{-38.9}$	2.58	281/214
3418	$0.52^{+0.01}_{-0.01}$	116^{+8}_{-5}	< 0.280	–	–	$6.361^{+0.033}_{-0.032}$	$88.0^{+29.0}_{-28.9}$	2.54	611/401
436	$1.03^{+0.03}_{-0.03}$	174^{+43}_{-37}	$713.6^{+34.7}_{-35.1}$	$0.87^{+0.02}_{-0.02}$	$0.21^{+0.02}_{-0.02}$	$6.340^{+0.092}_{-0.084}$	$61.6^{+83.4}_{-57.0}$	0.79	163/127
2319	$0.97^{+0.04}_{-0.04}$	125^{+67}_{-52}	$698.6^{+48.0}_{-48.3}$	$0.86^{+0.03}_{-0.03}$	$0.28^{+0.03}_{-0.04}$	$6.311^{+0.060}_{-0.047}$	$160.0^{+111}_{-94.7}$	0.93	93/64

[a] Absorption column density that does not include the Galactic contribution;

[b] Reflection scaling factor;

[c] Observed flux in 2–10 keV in units of 10^{-11} erg cm^{-2} s^{-1}.

5.1 Discussion

5.1.1 The Soft X-ray Emission

It is evident that the soft and hard X-rays are emitted from different regions in NGC 7582 and through different physical processes, as has been found in Xue et al. (1998) on the basis of a temporal analysis and in our X-ray imaging analysis (§4) and spectral analysis (§5) where the single power-law model gave poor fits. The excess seen in the soft X-rays can be accounted for by adding a Raymond-Smith spectral component, which indicates that there must be thermal gas in the central region of NGC 7582. This gas is most likely to be the product of violent starburst activities.

For NGC 2110, because of the pile-up effect, several soft X-ray photons detected in one frame time are counted as one single harder X-ray photon. Therefore, the X-ray count rate would have been biased in favour of the hard emission at the expense of the soft emission. This could explain why the observed X-ray spectra of NGC 2110 differed from those obtained in the previous missions, which showed excess soft X-ray emission below 1.2 keV.

5.1.2 The Flat Continuum

If fitted with a simple absorbed power-law model, both NGC 2110 and NGC 7582 show a flat spectrum in the X-ray band, which is consistent with the previous observations. The use of

more complicated models such as the dual absorbed and the reflection model can significantly raise the best-fitting power-law photon index. This result agrees with those obtained with *BeppoSAX* that have photon index $\Gamma = 1.97$ for NGC 2110 in 13–150 keV (Malaguti el al. 1999) and $\Gamma = 1.95$ for NGC 7582 in 2–100 keV (Turner et al. 2000). Therefore, we conclude that the intrinsic spectra of NGC 2110 and NGC 7582 are steep. They turn out to be flat because of the existence of additional absorbing matter.

A possible solution of the flat spectrum problem is the reflection model, which assumes that an intrinsically steep spectrum becomes flat because of contribution of hard photons reflected by the cold material. Zaziarski et al. (1999) pointed out that there is a strong correlation between the Compton reflection from the nucleus and the intrinsic photon index of the form $R = u\Gamma^{v}$, with model parameters u and v. In this case the reflection strength decreases with decreasing Γ. Since the Compton reflection plays an important role in cooling the thermal plasma where the soft X-ray photons are produced, less reflection should lead to less cooling, less soft X-ray photons, and hence a flatter spectrum. For NGC 2110 and NGC 7582, the reflection model does not give an obviously increased photon index, and the obtained reflection ratio R, which describes the relative strength of the reflection component, is too large for NGC 7582 ($R \approx 700$) and too small for NGC 2110 ($R \approx 0$).

We argue that the dual absorbed model is a more physically reliable model than the reflection model for both NGC 2110 and NGC 7582. When the X-ray emission from the nuclear region encounters the additional absorbing material, the hard X-ray photons can easily pass through, while the soft ones are heavily absorbed. As a result, intrinsically steep spectra become flattened. In this case, although the observations of NGC 2110 suffered from the pile-up effect, the best-fit photon index Γ still increased by 0.2. Our result is consistent with that from the *ASCA* observations (Xue et al. 1998).

5.1.3 The Fe K_α *Feature*

In the unified Seyfert theories, both the accretion disk and the molecular torus are expected to emit the Fe K_α lines. If the observed Fe K_α lines are produced in the molecular torus through transmission and/or reflection, then we can expect $EW \leq 40$ eV for a column density of $< 10^{23}$ cm^{-2} (Ghisellini, Haardt & Matt 1994). However, the measured equivalent widths are much larger than this value, indicating that the observed line cannot be explained only by the transmission in the torus. If we consider the contribution of an additional cold material as invoked in the dual absorbed model, the equivalent width of the line will be associated with the total column density $N_{\rm H}$. On the other hand, the reflection ratio R is too small for NGC 2110 and too large for NGC 7582 to produce the measured equivalent widths.

6 CONCLUSIONS

Our analysis of the *Chandra* observations of NGC 2110 and NGC 7582 has led to the following conclusions.

1. The high spatial resolution *Chandra* images show that the X-rays below 2 keV and in 2–10 keV are emitted from different regions in NGC 7582, confirming the result of Xue et al. (1998). By inspecting the spectra in different locations, the soft X-rays are found to be associated with regions where starburst activities take place.
2. Our temporal analysis did not show any significant variability in the X-ray flux of NGC 2110 and NGC 7582. However, because of the short exposure time and the pile-up effect, we

cannot exclude variability at low levels during our observations of these two galaxies.

3. The spectra of the two galaxies are apparently flat. The dual absorbed model which gives a better fit to the spectra, shows that the photon index of the power-law component is intrinsically steep. The additional absorption column density needed in the fit is consistent with the measured equivalent width of the Fe K$_\alpha$ line.

Acknowledgements We thank Dr. Hong-Yan Zhou for helpful discussions. This project is supported by NSFC (Grant number 10320130108) as well as by the Excellent Young Teachers Program of MOE, P. R. C.

References

Cappi M., Mihara T., Matsuoka M. et al., 1996, ApJ, 456, 141
Davis J.E., 2001, ApJ, 562, 575
Ghisellini G., Haardt F., Matt G., 1994, MNRAS, 267, 743
Guainazzi M., Matt G., Antonelli L. A., Fiore F., Piro L., Ueno S., 1998, MNRAS, 298, 824
Haardt F., Maraschi L., 1991, ApJ, 380, 51
Haardt F., 1993, ApJ, 413, 680
Haardt F., Maraschi L., 1993, ApJ, 413, 507
Hayashi I., Koyama K., Awaki H., Yamauchi S. U. S., 1996, PASJ, 48, 219
Lawrence A., Elvis M., 1982, ApJ, 256, 410
Magdziarz P., Zdziarski A. A., 1995, MNRAS, 273, 837
Malaguti G., Bassani L., Cappi M. et al., 1999, A&A, 342, 41
Malizia A., Bassani L., Zhang S. N. et al., 1999, ApJ, 519, 637
Mushotzhy R.F., 1982, ApJ, 256, 92
Nandra K., Pounds K.A., 1994, MNRAS, 268, 405
Polletta M., Bassani L., Malaguti G., Palumbo G. G. C., Caroli E., 1996, ApJS, 106, 399
Pounds K. A., Nandra K., Stewart G. C., George I. M., Fabian A. C., 1990, Nature, 344, 132
Risaliti G., 2002, A&A, 386, 379
Roche P. F., Whitmore B., Aitken D. K., Phillips M. M., 1984, MNRAS, 207, 35
Smith D.A., Done C., 1996, MNRAS, 280, 355
Stark A. A., Gammie C. F., Wilson R. W. et al., 1992, ApJS, 79, 77
Turner T.J., Pounds K.A., 1989, MNRAS, 240, 833
Turner T. J., Weaver K. A., Mushotzky R. F., Holt S. S., Madejski G. M., 1991, ApJ, 381, 85
Turner T. J., George I. M., Nandra K., Mushotzky R. F., 1997, ApJS, 113, 23
Turner T. J., George I. M., Nandra K., Mushotzky R. F., 1998, ApJ, 493, 91
Turner T. J., Perola G. C., Fiore F., Matt G., George I. M., Piro L., Bassani L., 2000, ApJ, 531, 245
Ueda Y., Ebisawa K., Done C., 1994, PASJ, 46, 107
Vignali C., Comastri A., Stirpe G. M. et al., 1998, A&A, 333, 411
Ward M., Penston M. V., Blades J. C., Turtle A. J., 1980, MNRAS, 193, 563
Warwick R. S., Sembay S., Yaqoob T. et al., 1993, MNRAS, 265, 412
Xue S. J., Otani C., Mihara T., Cappi M., Matsuoka M., 1998, PASJ, 50, 519
Zdziarski A. A., Fabian A. C., Nandra K. et al., 1994, MNRAS, 269, 55
Zdziarski A. A., Johnson W. N., Done C., Smith D., McNaron-Brown K., 1995, ApJ, 438, 63
Zdziarski A. A., Lubinski P, Smith D. A., 1999, MNRAS, 303, 11